The Aeronautical Journal (2024), **128**, pp. 1417–1428
doi:10.1017/aer.2024.39

ROYAL AERONAUTICAL SOCIETY

RESEARCH ARTICLE

Experimental investigation of a Y-shaped engine inlet at subsonic flow conditions

U.C. Küçük

Propulsion Aerodynamics, Turkish Aerospace, Ankara, Turkey
Email: kucukumutcan@gmail.com

Received: 15 July 2023; **Revised:** 13 February 2024; **Accepted:** 26 March 2024

Keywords: Aeroengine; wind tunnel tests; spectral analysis; engine integration; compatibility; inlet aerodynamics

Abstract

In this paper, the results of an experimental investigation for a Y-shaped engine inlet are presented. The experiment is performed at subsonic flow conditions. The main focus is given to time-dependent total pressures measured at the aerodynamic interface plane. Distinctive frequencies carrying high energy contents of the fluctuating total pressures are given and the relation between time-dependent and time-average performance parameters is presented. The cross-correlation coefficients of the high frequency probe readings distributed through the aerodynamic interface plane are also investigated.

Nomenclature

A_e	area of the engine face
A_{ent}	area of the inlet entrance
AIP	aerodynamic interface plane
AoA	angle-of-attack
ARA	Aircraft Research Association
AoS	angle of side slip
c	speed of sound
D	diameter
H	lateral offset
L	characteristic Length
M	Mach number
MDC	mean distortion
MFR	mass flow ratio
$\dot{m}$	mass flow rate
PR	pressure recovery
PT	total pressure
PDC	peak distortion
PSD	power spectrum density
P2P	peak to peak parameter
SAE	Society of Automotive Engineers
V	velocity
ρ	density
∞	free stream condition

A version of this paper first appeared at the 26th Conference of the International Society for Air Breathing (ISABE), 22–27 September 2024, Toulouse, France.

1.0 Introduction

Engine inlets are designed to respond to engine mass flow demand with minimum total pressure loss and maximum flow uniformity. Total pressure loss has a direct effect on the thrust and fuel consumption rate [1]. On the other hand, increasing non-uniformity at the engine face leads to stability margin reduction which is well understood and can be modeled with parallel compressor theory [2, 3]. It is also well-recognised that pressure fluctuations at the engine face can have a detrimental effect on the engine stability characteristics [4, 5] as well. These pressure fluctuations may originate from internal and external disturbances. External disturbances include boundary layer separation occurring upstream of the inlet entrance, shock-boundary layer interactions, wakes or vortex originating from landing gear, aircraft nose and other upstream protuberances. Flow separation, secondary flows created by the strong curvatures and high adverse pressure gradients inside the inlet may also trigger the pressure fluctuations. Therefore, both internal and external flow characteristics play a major role in reaching the successful integration of the air-breathing engine into the aircraft.

Diffusing Y-shaped engine inlets, having two identical entrances discharging to a common exit, are commonly used in aircraft applications. Although these inlet designs are proven to be successful in satisfying the engine mass flow demand, these inlets can bring design challenges. At the end of the first decade of the jet-propelled aircraft design, it is shown that these inlets are prone to flow instabilities, and it is further shown that the instability is a strong function of static pressure variation at the juncture of the two ducts [6]. These instabilities bring flow asymmetry and high levels of pressure fluctuations at the engine face. The effect of this flow asymmetry can be detrimental even on the stability and flight characteristics of the aircraft [7]. Seddon and Trebble [8] observed the asymmetrical flow behaviour of a typical Y-shaped inlet located at the wing root of an aircraft. They commented that the asymmetric flow can be observed in a dive or when mass flow is reduced. Sudhakar and Ananthkrishnan [9] explained the phenomenon that triggers the asymmetrical operation condition. They mathematically explained that asymmetry can occur when the pressure recovery variation with respect to the mass flow rate has a maximum. More recently flow asymmetry in a Y-shaped diverterless inlet at supersonic flow conditions is documented [10]. Although the flow unsteadiness and instability on several engine inlet development programs are also reported in the literature [11–14], the flow physics when the instability occurs is yet to be understood. There are a number of studies investigating the unsteady flow mechanism. In such a study conducted by MacManus et al. [15], the unsteady flow field for several diffusers with centre line curvature is computationally investigated and levels of total pressure distortion as well as swirl for the investigated ducts are presented. In another study [16], unsteady swirl distortions for two diffuser configurations with different centreline offsets are measured using stereoscopic particle image velocimetry. Results indicate that the high offset duct leads to a higher swirl distortion.

The flow asymmetry and flow unsteadiness observed in Y-shaped inlet ducts for low subsonic to supersonic conditions are well documented. However, there is not much information about the frequency content investigation of the total pressure fluctuations. Accordingly, in this study, this gap tried to be filled with the experimentally obtained total pressures for a Y-shaped intake at a range of flow conditions. Observations regarding the flow characteristics at the aerodynamic interface plane with inlet performance parameters which are known to have a significant effect on the engine-inlet compatibility are also discussed.

2.0 Model and wind tunnel tests

The model size is scaled to 1/7th of the full-scale aircraft to create only an acceptable level of blockage in the test section and to use the existing mass flow plug. The model includes aircraft nose, wing leading edge extension and inlet ducts as shown in Fig. 1. The aerodynamic surfaces on the model have surface roughness smaller than 32 micrometers. Model deviation tolerances are kept below 0.12 mm on the forebody, internal and external faces of the duct including the inlet lips.

The inlet duct has typical properties of a Y-shaped duct with only negligible vertical offset distance between centroids of the inlet entrance and aerodynamic interface plane (AIP). The AIP is historically

https://doi.org/10.1017/aer.2024.39 Published online by Cambridge University Press

Table 1. *Geometrical parameters of the Y-shaped duct*

$A_e/2A_{ent}$	L/D	H/D
1.3	5.5	1.2

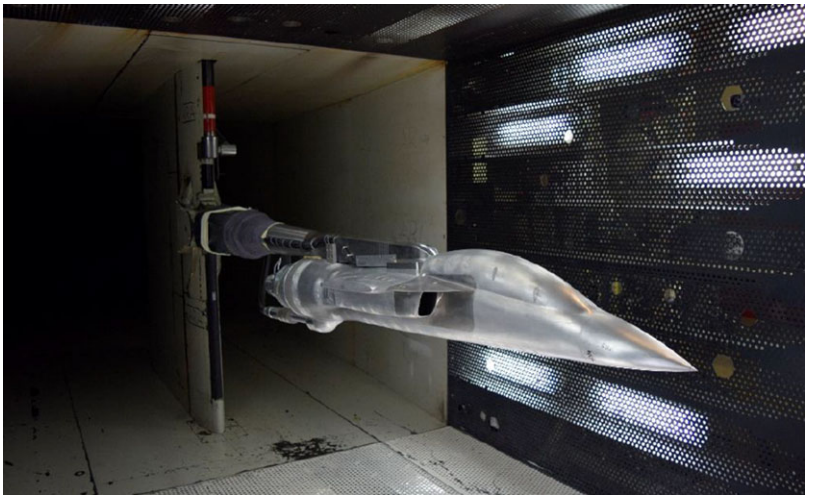

Figure 1. *Test model in the test section.*

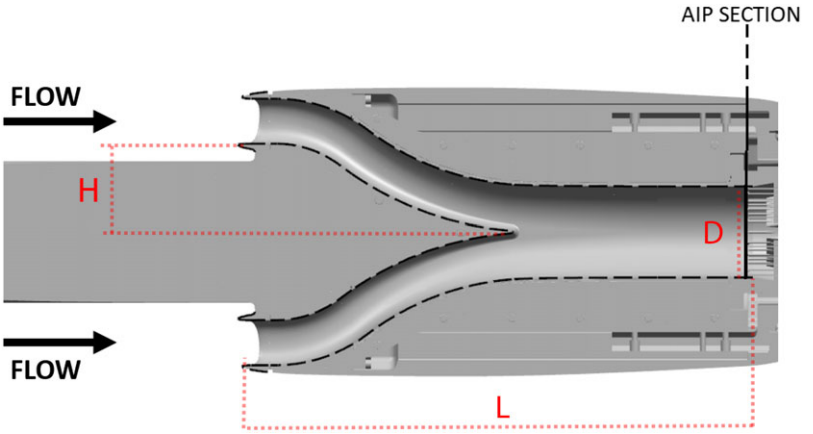

Figure 2. *Mid-plane cut view from top.*

defined as a hypothetical plane located just upstream of the engine face where information about the engine inflow conditions is obtainable. In this work, the AIP is located in accordance with the historical approach. The inlet has a boundary layer diverter between the fuselage and the inlet entrance whereas the inlet entrance is flush-mounted to the leading edge extension.

The geometrical properties of the investigated inlet are given in Table 1 where A_e is the AIP area and A_{ent} is the inlet entrance area enclosed with the leading edge of the inlet lips. The top view of the investigated model at the mid-plane is also given in Fig. 2.

The test is conducted in ARA 8ft × 9ft transonic wind tunnel in Bedford, UK. Dual-purpose Kulites, which can provide low and high-frequency measurements, are used at the AIP. The number of probes and

https://doi.org/10.1017/aer.2024.39 Published online by Cambridge University Press

Table 2. *Flow conditions*

M_∞	AoA°	AoS°
0.5, 0.8, 0.95	–3°, 0°, 6°	0°

their orientation are decided in accordance with SAE standard [17]. Therefore, 40 probes are located at the AIP in 8 rakes each carrying 5 probes at the centroids of equal areas. Kulite XCP-110-25SG, which provides both low and high-frequency measurements, is used in the total pressure rake and data is collected with 25 khz. These probes provide low uncertainty (0.5%).

The amount of the ingested mass flow rate by the intake is determined with the pre-calibrated mass flow plug. During the operation of the mass flow plug it is always ensured that the mass flow plug is working in chocked condition so that the reflection plane of the engine is well simulated. At low Mach number test conditions ejectors are used to reach the representative mass flow rates whereas at the high Mach number conditions, ejectors are not required. Tests are conducted with move-and-pause methodology so that the model is oriented at the desired attitude and then data is taken only after a pre-determined flow settling duration. The flow conditions that are focused on in this study are given in Table 2.

3.0 Inlet performance parameters

The key performance parameters that are focused on in this study are to correlate dynamic and time-averaged behaviours of the Y-shaped duct. The level of the inlet unsteadiness is quantified with the peak-to-peak parameter (see Equation (1)) which simply measures the amplitude of the total pressure fluctuations compared to the mean total pressure at the AIP.

$$P2P = \frac{\left(max\left(PT_{AIP,k}\right) - min\left(PT_{AIP,k}\right)\right)}{PT_{AIP,ave}} \tag{1}$$

Where $PT_{AIP,k}$ shows the instantaneous rake average total pressure at the kth sample and $PT_{AIP,ave}$ is the time average of the rake total pressure for the whole data acquisition duration.

Additionally, peak and mean distortion parameters are investigated to measure time-dependent and mean total pressure uniformity at the AIP. The definitions of these distortion parameters are given in Equations (2) and (3) for peak (maximum time variant) and mean (time average) distortions respectively.

$$PDC = max\left(\frac{PT_{AIP,k} - PT_{i,k}}{PT_{AIP,k}}\right) \tag{2}$$

$$MDC = \frac{PT_{AIP,ave} - PT_{min}}{PT_{AIP,ave}} \tag{3}$$

Where $PT_{i,k}$ is the kth sample of the total pressure reading from the ith probe and PT_{min} is the minimum of the time average values of the total pressure readings from the individual probes of the AIP rake. P2P and distortion values are further normalised with their maximums obtained within the investigated flow conditions.

Similarly, the pressure recovery of the inlet calculated from Equation (4) is obtained from time average total pressure measurements.

$$PR = \frac{PT_{AIP,ave}}{PT_\infty} \tag{4}$$

where PT_∞ is the free stream total pressure in the test section. Pressure recovery values are further normalised with the minimum obtained from the investigated flow conditions. Accordingly, in the rest of the study, only the normalised values of P2P, PDC, MDC and PR are given.

https://doi.org/10.1017/aer.2024.39 Published online by Cambridge University Press

The mass flow ratio which simply measures the relative size of the captured tube compared to the highlight area is calculated from equation Equation (5).

$$MFR = \frac{\frac{\dot{m}}{\rho_\infty V_\infty}}{A_{ent}} \tag{5}$$

where A_{ent} is the inlet entrance area of the individual duct.

4.0 Results and discussion

The time-dependent total pressures are experimentally obtained at the AIP for a typical Y-shaped duct at subsonic flow conditions. Results indicate an increasing flow unsteadiness with a decrease in mass flow rate. The effect of the increased unsteadiness on the time-dependent and time-average performance parameters of the engine inlet is investigated first for the flow conditions given in Table 2. Next, a flow asymmetry seen in the investigated conditions is briefly discussed. Frequency analyses of the pressure fluctuations are also conducted to determine dominant frequencies with high energy content at the 0 ° angle-of-attack conditions.

4.1 Observation on the performance parameters

The key performance parameters of the investigated flow conditions are shown in Fig. 3. The first thing noted from this figure is the change in flow characteristics after reduction from a certain mass flow ratio (MFR) shown with vertical dotted lines. Further reduction from this MFR level leads to an increase in duct losses indicated by a reduction in pressure recovery (PR). The increase in losses is also accompanied by a general increase in the flow unsteadiness and a change in the dependency of the distortion on the mass flow rate. Accordingly, the MFR value of which PR starts to decrease with decreasing MFR is defined as the critical MFR. This critical MFR value is a strong function of the angle-of-attack whereas it is only a weak function of Mach number. As the angle-of-attack increases the critical MFR value decreases whereas a change in Mach number has only negligible effect on the critical MFR value. In other words, for a given angle-of-attack, the critical MFR is almost independent of the Mach number. This indicates that the triggering mechanism of the flow unsteadiness is mostly related to the size of the ingested stream tube characterised by MFR and its interaction with the external surfaces of the aircraft.

Investigation of Fig. 3 reveals that; below the critical MFR value, PR values start to decrease with decreasing MFR. The decrease in PR can reach up to 4% of its peak value obtained at the critical MFR for the investigated flow cases. The magnitude of the decrease in PR and the magnitude of the increase in flow unsteadiness are directly correlated with each other, indicating losses increase the flow unsteadiness for the Y-shaped inlet. A similar correlation between the level of distortion and flow unsteadiness can be obtained from Fig. 3. For the conditions at which flow unsteadiness is low both the time average and peak distortion levels are close to each other and they show a decreasing trend with a decrease in MFR level. However, as the flow unsteadiness increases the relative difference between time-averaged and maximum time variant distortion levels also increases and peak distortion levels become considerably (up to 3 times) higher compared to the time average distortion levels. Additionally, when the flow unsteadiness is relatively high, there is a range of MFR levels at which a decrease in MFR leads to an increase in both time average and peak distortion levels. This is due to fluctuating pressures with higher amplitude and increased losses.

From the above discussions, it can be summarised that the positive slope of pressure recovery and the negative slope of the distortions with increasing MFR, which can also be obtained from time-averaged data, are clear indications of increasing flow unsteadiness inside the Y-shaped duct. The information obtained only from the low-frequency instrumentation can be used for evaluating the time-dependent characteristics of the inlet so that low-cost test campaigns can be planned especially in the early design phases. The lower-cost instrumentation may provide longer test runs or an increased number

https://doi.org/10.1017/aer.2024.39 Published online by Cambridge University Press

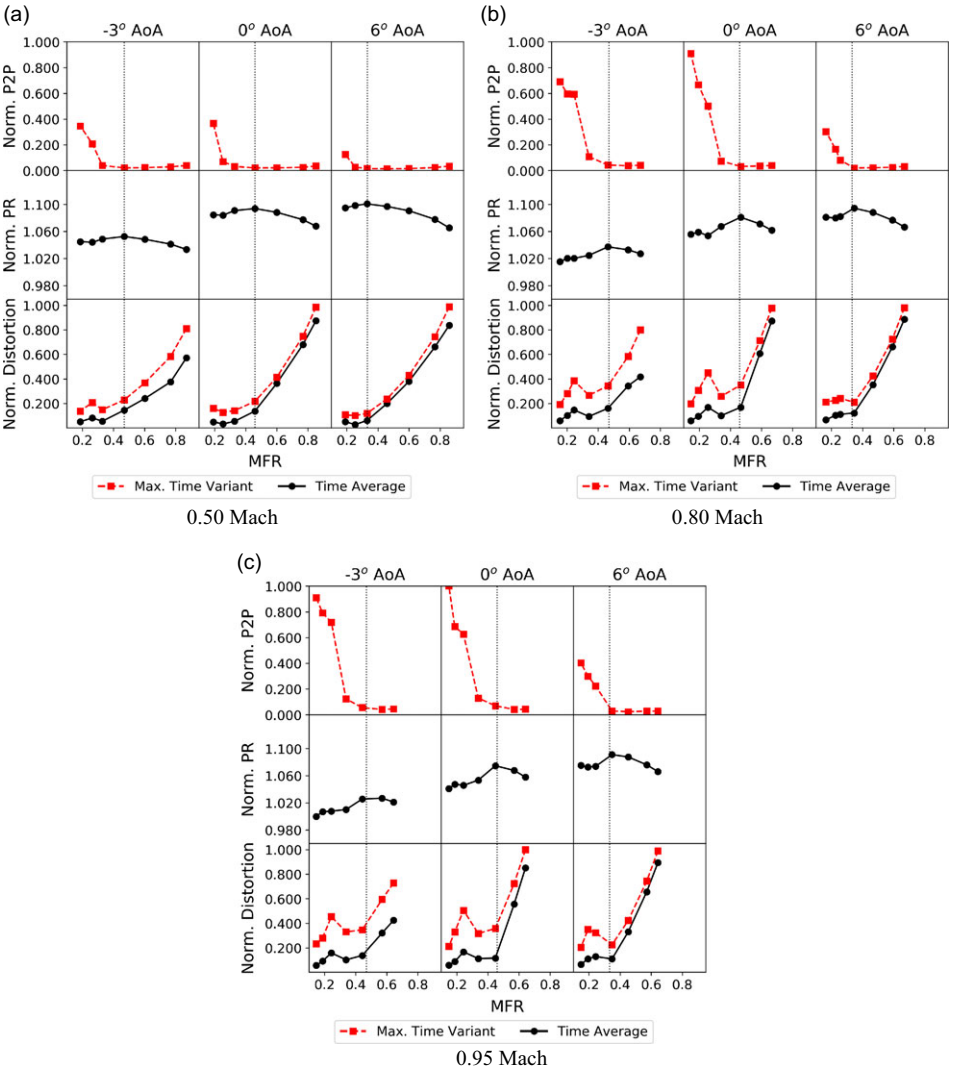

Figure 3. *Inlet performance parameters.*

of geometrical configurations investigated in the wind tunnel so that the relative effect of design changes on the inlet dynamic characteristics can be investigated in a broader sense.

4.2 Flow asymmetry

Investigating the characteristics of the pressure recovery distributions at the AIP results in an interesting observation; below the critical MFR value of which PR starts to decrease with decreasing MFR for a given free stream Mach number and model attitude, total pressure distributions indicate flow asymmetry in the Y-shaped duct. The observation is given in Fig. 4. As seen, regardless of the Mach number investigated, low total pressure sectors at the two sides of the AIP occur for the highest mass flow ratios. This is mostly due to the flow separated from the outer walls of the inlet. As the MFR reduces, the losses decrease until the critical value so that low total pressure sectors at the two sides become insensible. Further reduction in the MFR levels increases losses and introduces a low total pressure region at one side of the AIP so flow asymmetry is introduced for each of the investigated conditions. It is also

https://doi.org/10.1017/aer.2024.39 Published online by Cambridge University Press

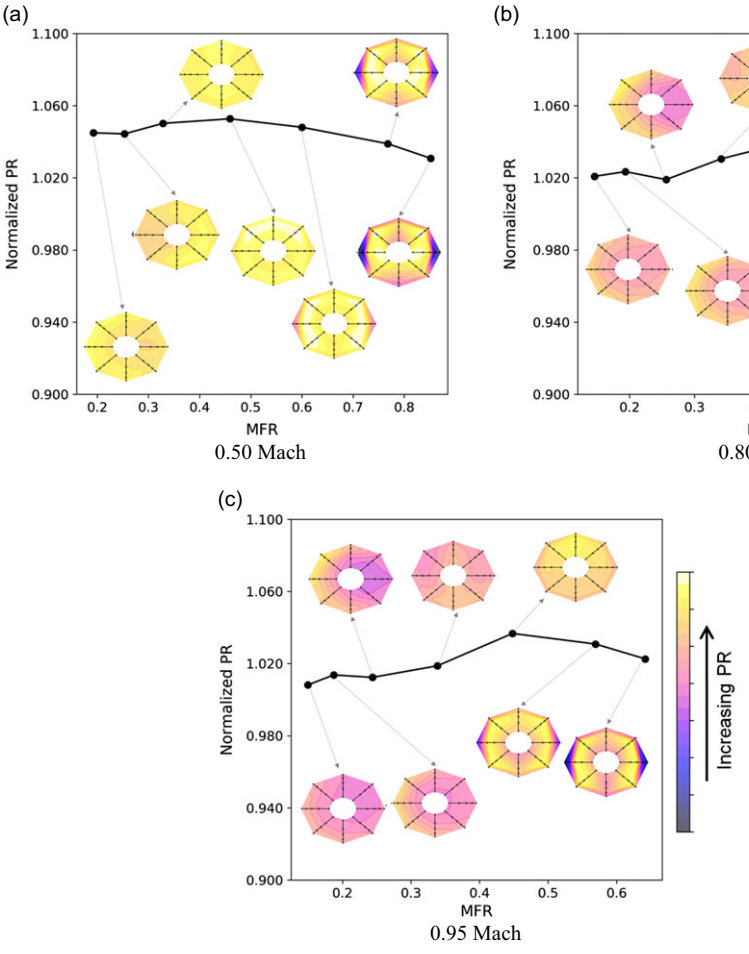

Figure 4. *Total pressure distribution change at the AIP for different levels of mass flow ratios at 0° AoA and AoS.*

interesting to note that, for the free stream Mach number of 0.5, the low total pressure sector seen in low MFR values moves from one side to the other. Additional high-frequency pressure measurements within the duct may explain the reason behind this phenomenon.

4.3 Unsteady flow

The power spectral density (PSD) is a powerful tool for understanding the distinctive frequencies and their energy content by distributing the mean squared value of pressure in the frequency domain. The PSD plots, which are obtained with Welch method [18], are given in Figs 5–7 for the investigated free stream Mach numbers to observe dominant frequencies and the energy levels of different frequencies in the Y-shaped duct. From these figures, it is seen that at conditions with relatively high MFR, the energy levels of the fluctuating pressures are homogeneously distributed through the investigated frequency range. As the MFR value decreases the energy levels of the pressure fluctuations increase and distinctive frequencies carrying the highest energy levels become visible. First distinctive frequencies around 90 Hz and 500 Hz become visible then with the further decrease in MFR, additional peaks around 270 Hz, 650 Hz and 1,050 Hz start to be seen.

https://doi.org/10.1017/aer.2024.39 Published online by Cambridge University Press

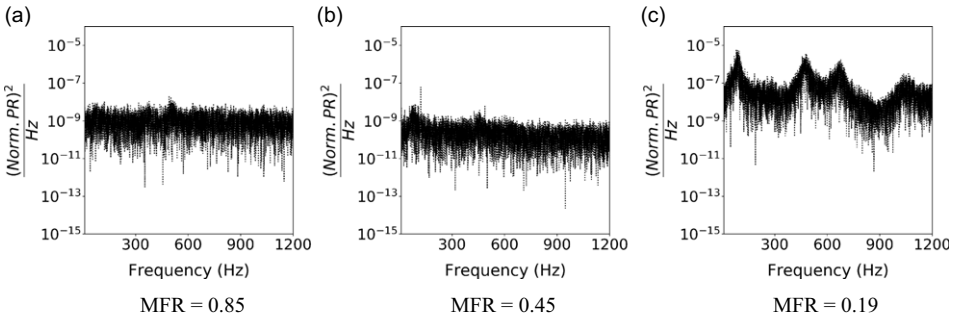

Figure 5. *PSD plots at 0.50 Mach, 0° AoA and AoS.*

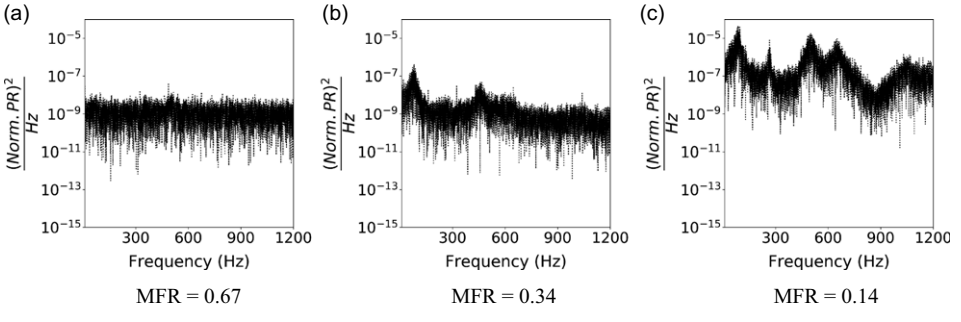

Figure 6. *PSD plots at 0.80 Mach, 0° AoA and AoS.*

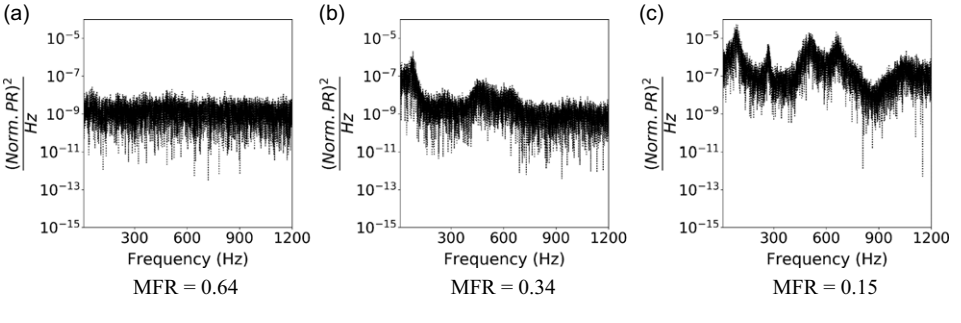

Figure 7. *PSD plots at 0.95 Mach, 0° AoA and AoS.*

It is known that the distinctive frequencies of the fluctuations are directly related to the resonance modes for a duct with open and closed ends. Equation (6) [19] can be applied for distinctive frequencies of a duct with open and closed ends.

$$F_n = (2n+1)\left(\frac{c}{4L}\right)\left(1-M^2\right) \quad n = 1, 2, 3, .. \tag{6}$$

where L is the total length of the duct starting from the leading edge of the inlet lips up to the chocking plane at the mass flow plug, c speed of sound and M is the calculated Mach number in the duct. This formulation is mostly used for supersonic inlet buzz which is known as the self-sustained oscillation of shock waves leading to high amplitude of pressure fluctuations. In most of the cases, flow separation at the upstream of the supersonic inlet triggered by the shock wave-boundary layer interaction is associated with the inlet buzz. The process leads to the flow unsteadiness for the Y-shaped inlet is similar even

https://doi.org/10.1017/aer.2024.39 Published online by Cambridge University Press

Table 3. *Calculated and observed frequencies at 0.95 Mach, 0° AoA and AoS*

	$n=0$	$n=1$	$n=2$	$n=3$	$n=4$	$n=5$
Calculation	92	275	459	643	826	1,010
Observation	87	270	501	657	–	1,057

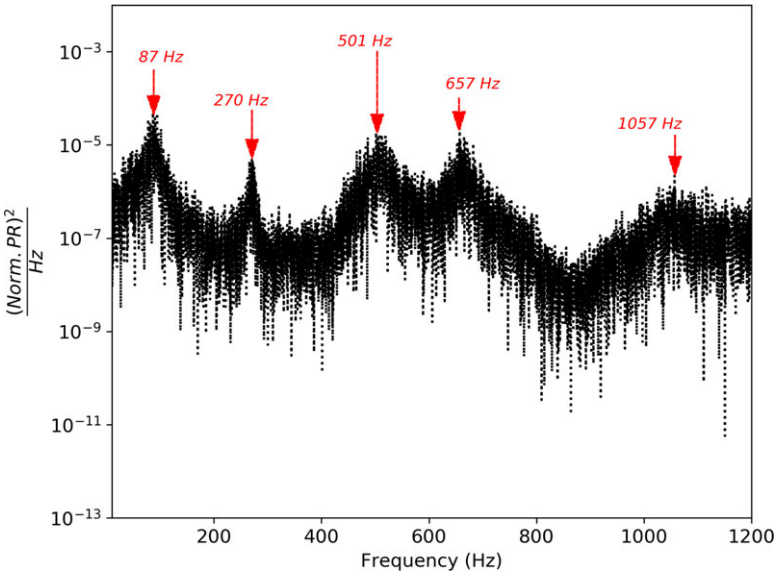

Figure 8. *Distinctive frequencies at 0.95 Mach, 0° AoA and AoS.*

for subsonic conditions although the expected amplitudes are much smaller compared to the typical supersonic buzz. Accordingly, acoustic frequencies calculated from Equation (6) are compared with the dominant frequencies observed from the experimental data. In an earlier study [20], it is shown that the discrete frequencies carrying the highest energy levels have good agreement with the fundamental resonance modes for a single inlet at a free stream Mach number of 0.85. To the author's best knowledge results of a discrete frequency investigation are first given herein for a Y-shaped engine inlet in which flow is inherently highly three-dimensional and includes asymmetry.

Investigation of the wind tunnel data indicates that calculated and observed acoustic frequencies agree well with each other (see Table 3). The observed frequencies for a free stream Mach number of 0.95 are closely shown in Fig. 8. Interestingly fourth acoustic resonance mode of the duct has not occurred. More interestingly, the frequency at which the fourth mode is calculated to occur corresponds to a 'silent' region for each of the investigated conditions (see Figs 5–8). The reason behind such characteristics is left unclear to the author.

Another observation regarding the flow unsteadiness captured from the pressure fluctuations at the AIP is related to the behaviour of the individual high-frequency total pressure probes. It is observed that as the level of unsteadiness increases the behaviour of the individual probes becomes correlated to each other independent of model attitude and free stream Mach number. Generally, probe measurements have some correlation of practical significance if the length scale of the flow structure measured by the two probes is comparable to the distance between the probes. The significance level of the correlation between two probes can be quantified with a cross-correlation coefficient which measures the dependence of the pressure measurement from a probe at an instant with the pressure measurement from another probe at another instant. Accordingly, the inner probe at the third rake is arbitrarily selected and the cross-correlation coefficient between this selected probe and three probes with different distances are calculated. This selection is to present the effect of the varying distances between the probes on

https://doi.org/10.1017/aer.2024.39 Published online by Cambridge University Press

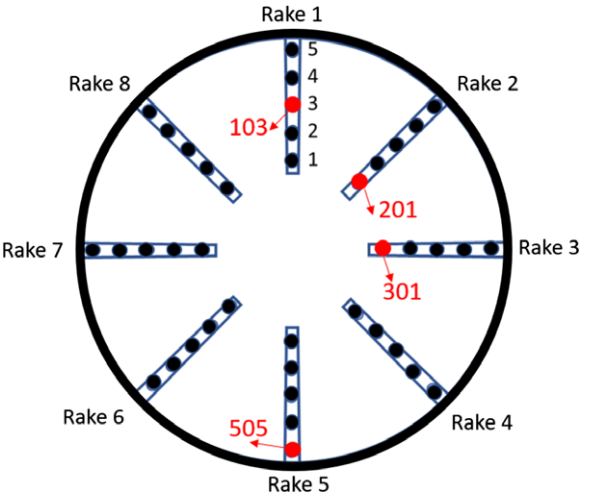

Figure 9. *Location of the selected probes for cross-correlation coefficient investigation.*

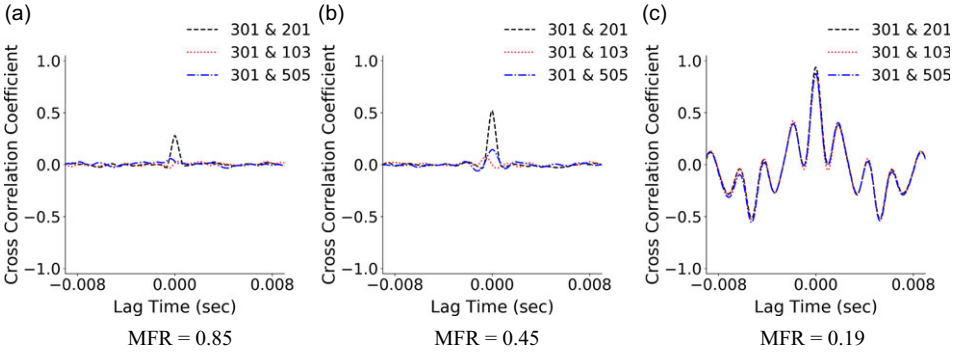

Figure 10. *Cross correlation coefficients for selected probes at 0.50 Mach, 0° AoA and AoS.*

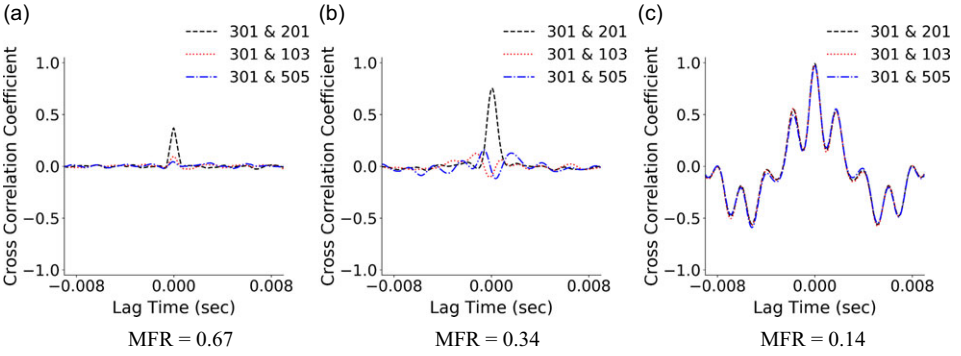

Figure 11. *Cross correlation coefficients for selected probes at 0.80 Mach, 0° AoA and AoS.*

the correlation coefficients. The conclusions drawn will be the same for different probes with comparable distances. The locations of the selected probes for the cross-correlation calculations are given in Fig. 9 whereas the calculated cross-correlation coefficients of these probes are given in Figs 10–12. From these figures, it is seen that there is always some level of correlation between the closely located probes. However, as the distance between the probes is increased, their behaviour becomes independent

https://doi.org/10.1017/aer.2024.39 Published online by Cambridge University Press

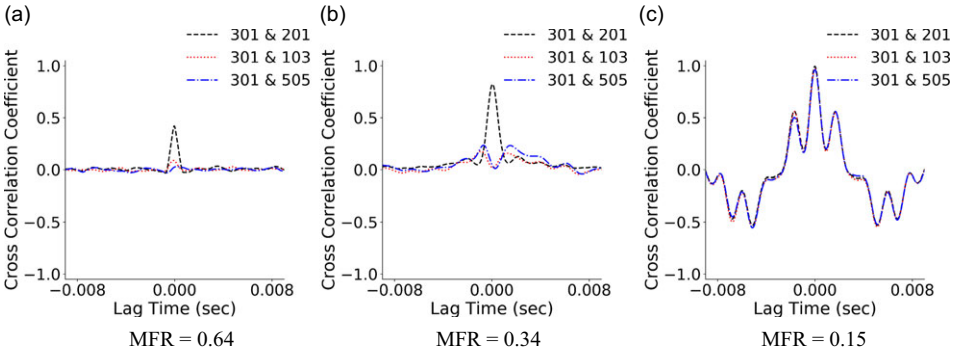

Figure 12. *Cross correlation coefficients for selected probes at 0.95 Mach, 0° AoA and AoS.*

for relatively high mass flow conditions. As the flow unsteadiness increases the correlation coefficient reaches almost one independent of the distance between the probes, which indicates a strong correlation. This can be attributed to the typical characteristics of the planar wave so that the size of the eddies becomes comparable to the diameter of the AIP as the flow unsteadiness increases.

From the given observations, it can be commented that a rake with 40 high-frequency total pressure probes is more than sufficient if only the item of interest is defining planar wave onset for a given inlet. Cross-correlation coefficients obtained from a smaller number of high-frequency probes distributed on the AIP rake may provide sufficient information for determining the range of stable operating conditions.

5.0 Conclusion

In this study, experimental observations related to the flow characteristics of a typical Y-shaped duct in subsonic flow conditions are commented. Observations mainly depend on the high-frequency total pressure readings obtained at the aerodynamic interface plane. Results indicate that:

1. A decrease in pressure recovery and an increase in distortion with decreasing MFR are clear indications of the flow unsteadiness inside a Y-shaped duct. The variation of the time average values of the pressure recovery and distortion can be used as an indication of an increase in the flow unsteadiness.
2. The condition at which the flow unsteadiness becomes more pronounced is a strong function of the size of the ingested stream tube characterised by MFR rather than the free stream Mach number. On the other hand, the magnitude of the flow unsteadiness is a direct function of the flow conditions.
3. Flow asymmetry is observed below critical MFR with increasing flow unsteadiness. Additional high-frequency pressure readings inside the duct may provide a further understanding of the possible triggering factor of this flow asymmetry.
4. Investigation of the dominant frequencies indicates that as the flow unsteadiness increases, frequencies with the zeroth and second fundamental modes of the duct start to be seen. Then with the further increase in flow unsteadiness other fundamental frequencies become observable. The calculated and observed fundamental frequencies have good agreement with each other. However, fourth fundamental mode is not observed in any of the investigated flow conditions.
5. The calculated cross-correlation coefficients of the probes distributed on the AIP reveal that the pressure readings of the probes become highly correlated when unsteadiness is significant. The size of the eddies becomes comparable to the diameter of the AIP at the conditions with a high level of flow unsteadiness. This indicates that a small number of high-frequency probes distributed on the AIP may provide sufficient information for determining the range of stable operating conditions for a given inlet.

https://doi.org/10.1017/aer.2024.39 Published online by Cambridge University Press

Acknowledgements. The author wishes to thank Turkish Aerospace for allowing this work to be published.

References

[1] Sóbester A. Tradeoffs in jet inlet design: a historical perspective. *J. Aircraft*, 2007, **44**, (3), pp 705–717.
[2] Pearson H. and McKenzie A. B wakes in axial compressors. *Aeronaut. J.*, 1959, **63**, (583), pp 415–416.
[3] Mazzawy R.S. Multiple segment parallel compressor model for circumferential flow distortion. *ASME. J. Eng. Power*, 1977, **99**, (2), pp 288–296.
[4] Williams D.D. and Yost J.O. Some aspects of inlet/engine flow compatibility. *Aeronaut. J.*, 1973, **77**, (753), pp 483–492.
[5] Ball W.H. Inlet planar waves: a current perspective. *Proceedings of the ASME 1991 International Gas Turbine and Aeroengine Congress and Exposition. Volume 2: Aircraft Engine; Marine; Microturbines and Small Turbomachinery*, American Society of Mechanical Engineers (ASME), June 3–6, 1991, p V002T02A044.
[6] Martin N.J. and Holzhauser C.A. Analysis of factors influencing the stability characteristics of symmetrical twin-intake air-induction systems. NACA- Report TN-2049, 1950.
[7] Anderson W.E. and Perkins E.W. Effects of unsymmetrical AirFlow characteristics of twin-intake air-induction Systems on Airplane Static Stability at Supersonic Speeds. NACA- Report TM-X-942049, 1959.
[8] Seddon J. and Trebble W. *Model Test on the Asymmetry of Airflow Occurring in Twin-Intake Systems at Subsonic Speeds*. London: Aeronautical Research Council Repts. and Memoranda 2910, 1955.
[9] Sudhakar K. and Ananthkrishnan N. Jump phenomena in Y-shaped intake ducts. *J. Aircraft*, 1996, **33**, (2), pp 438–439.
[10] Askari R. and Soltani M.R. Flow asymmetry in a Y-shaped diverterless supersonic inlet: a novel finding. *AIAA J.*, 2020, **58**, (6), pp 2609–2620.
[11] Ki D. and Lee Y. An experimental study on the intake boundary layer diverter heights for transonic aircraft. *34th AIAA/ASME/SAE/ASEE Joint Propulsion Conference and Exhibit*, American Institute of Aeronautics and Astronautics (AIAA), 1998, p 3581.
[12] Hall G., Hurwitz W., Tiebens G, Norby W., Singshinsuk P. and Wilt C. Development of the F/A-18 E/F air induction system. *29th Joint Propulsion Conference and Exhibit*, American Institute of Aeronautics and Astronautics (AIAA), 1993, p 2152.
[13] Philhower J., Robinson D. and Brown R. Development of a highly offset induction system for a supersonic STOVL fighter. *34th AIAA/ASME/SAE/ASEE Joint Propulsion Conference and Exhibit*, American Institute of Aeronautics and Astronautics (AIAA), 1998, p 3417.
[14] Ramachandra S.M., Sudhakar K., Perumal P.V.K. and Jayasimha P. Air-Inlet engine matching problems encountered in a jet trainer re-engining program. *J. Aircraft*, 1982, **19**, (8), pp 609–614.
[15] MacManus D.G., Chiereghin N., Prieto D.G. and Zachos P.K. Complex aeroengine intake ducts and dynamic distortion. *AIAA J.*, 2017, **55**, (7), pp 2395–2409.
[16] Gil-Prieto D., MacManus D.G., Zachos P.K., Tanguy G. and Menzies K.R. Convoluted intake distortion measurements using stereo particle image velocimetry. *AIAA J.*, 2017, **55**, (6), pp 1878–1892.
[17] Society of Automotive Engineers. Gas turbine engine inlet flow distortion guidelines. Society of Automotive Engineers Report SAE ARP1420, 1978.
[18] Welch P. The use of fast Fourier transform for the estimation of power spectra: a method based on time averaging over short, modified periodograms. *IEEE Trans. Audio Electroacoust.*, 1967, **15**, (2), pp 70–73.
[19] Newsome R.W. Numerical simulation of near-critical and unsteady, subcritical inlet flow. *AIAA J.*, 1984, **22**, (10), pp 1375–1379.
[20] Macmiller C. and Haagenson W. Unsteady inlet distortion characteristics with the B-1B. *Paper presented at the 68th(A) Specialists Meeting of the AGARD Propulsion and Energetics Panel on Engine Response to Distorted Inflow Conditions*, AGARD, Munich, Germany, September 8–9, 1986.

Cite this article: Küçük U.C. (2024). Experimental investigation of a Y-shaped engine inlet at subsonic flow conditions. *The Aeronautical Journal*, **128**, 1417–1428. https://doi.org/10.1017/aer.2024.39